Aerospace Science and Technology 14 (2010) 387–396

Contents lists available at ScienceDirect

Aerospace Science and Technology

www.elsevier.com/locate/aescte

# Satellite orbit determination using a batch filter based on the unscented transformation

Eun-Seo Park, Sang-Young Park *, Kyoung-Min Roh, Kyu-Hong Choi

*Astrodynamics and Control Laboratory, Department of Astronomy, Yonsei University, Seoul 120-749, Republic of Korea*

ARTICLE INFO

*Article history:*
Received 22 January 2008
Accepted 24 March 2010
Available online 1 April 2010

*Keywords:*
Unscented transformation
Batch filters
Satellite orbit determination

ABSTRACT

In this paper, the non-recursive batch filter has been presented and utilized for satellite orbit determination. Using the unscented transformation, the non-recursive batch filter is developed without any traditional linearization process. For the orbit determination system, the range, azimuth, and elevation angles of the satellite measured from ground tracking stations are used for observations. For evaluation and verification of the presented batch filter's performance, the results are compared with those of the batch least squares filter for various initial errors in position and velocity, measurement sampling periods and measurement errors. For relatively small initial errors or short measurement sampling periods or small measurement errors, the accuracy of the orbit determination is similar in both the filters. Under large initial errors or long measurement sampling periods or large measurement errors, the presented non-recursive batch filter yields more robust and stable convergence than the existing batch least squares filter. The non-recursive batch filter based on the unscented transformation is effectively applicable for highly nonlinear batch estimation problems.



## 1. Introduction

There are two general categories of estimators: batch filters and sequential filters. The batch filter collects all the data for a fixed period and processes it together non-recursively. The sequential filter sequentially or recursively updates the state vector to produce a better estimate at each epoch [9]. The batch filter is commonly employed for off-line applications such as precise orbit determination for satellite. On the other hand, in on-line applications, i.e. on-board navigation of satellite in real time, the sequential filter is typically used for the estimation algorithm. For the off-line applications, the batch least squares method has the advantages of providing state estimation with a smaller error than a sequential filter like the extended Kalman filter (EKF). The batch filter is extremely helpful when accuracy is an issue [4]. However, when a real-time application is required, the EKF needs less memory storage and processor time than the batch least squares method because it does not demand iterations [20]. Although the batch least squares estimation and the EKF are the most widely used for solving nonlinear parameter estimation problems [2,3,5,9,11,19,20], they have some flaws due to the linearization process. Typically, both the methods are applied to nonlinear systems by simply linearizing and approximating all the nonlinear models. For the orbit determination, the dynamic system is linearized about reference trajectory with the assumption that the reference trajectory is very close to the true trajectory. This linearization in the batch least squares filter and the EKF may cause a large error, instability and divergence in the estimation process when the initial reference trajectory condition is not accurate and the measurement data are sparse or insufficient [13].

To overcome these problems, a number of algorithms have been developed, such as the unscented Kalman filter (UKF) [10], particle filters [6], the exact nonlinear recursive filters [6], and so forth. In particular, the UKF has been extensively investigated for its use with various dynamics systems, including determining a satellite attitude [5] or its orbit [12,13] or the trajectory of ballistic missiles [7]. Such research has shown that the UKF yields superior performance in highly nonlinear situations because the UKF is based on the unscented transformation which doesn't contain any traditional linearization processes or assumptions. This characteristic makes the UKF insensitive to the uncertainty of the initial guessing process. However, these approaches are just used for the real-time sequential or recursive filters, and not for the non-recursive batch estimations. The motivation of the current research is to develop a non-recursive batch filter without any traditional linearization processes using the unscented transformation.

There are other methods for nonlinear estimation, the so-called iterative or smoothing filters. To estimate the states and parameters, these filters use the batch set of measurement data for fixed interval and a combination of two filters. One of the two filters works forward over the data and the other of which runs backward over the interval [8]. The EKF is usually used to accomplish

* Corresponding author.
*E-mail address:* spark@galaxy.yonsei.ac.kr (S.-Y. Park).

1270-9638/$ – see front matter 
doi:10.1016/j.ast.2010.03.007

this task. The existing iterative EKF or EKF smoother [1] and other extension methods for iterative or smoothing principles [15] still have linearization problems. As alternative methods, smoother algorithms based on the unscented transformation are developed and utilized for satellite attitude determination [16] and tracking of a ballistic target [23]. However, these iterative or smoothing filters process the measurement sequentially because sequential filters, like EKF or UKF, are used for forward or backward pass procedures.

The first goal of the current research is to present the alternative algorithm of the non-recursive batch filter based on the unscented transformation, a method for calculating the statistics of a random variable which undergoes a nonlinear transformation [10]. The proposed algorithm (we call it non-recursive unscented batch filter) estimates system states and parameters at a chosen epoch time non-recursively using the batch set of data collected in total acquisition time, which is different to iterative or smoothing filters that have a recursive or sequential process for measurement data in forward or backward smoothing. The basic batch filter based on the UT is presented in our previous research and it is implemented to the attitude determination of satellite [17]. It shows that the batch filter based on the UT gives a fewer iterations for convergence than does the batch least squares filter. Also, the achieved accuracies obtained from the presented batch filter are similar or a bit better than those of the batch least squares filter even though the difference is within $1\sigma$ error [17]. The attitude sensors (rate-integrating gyro and three-axis magnetometers) can obtain measurement data continuously. However, the orbit determination system using the measurement of ground tracking stations is difficult to get continuous measurement data due to the geometrical relations between satellites and stations. In other words, the tracks are widely separated and the measurement data are very sparse. In this condition, the nonlinearity effects are strengthened. Thus it is very challenged that the performance of the proposed algorithms can be analyzed in detail using very nonlinear measurements. So, the second goal of the current research is to apply the non-recursive unscented batch algorithm to the orbit determination of a low Earth orbiting satellite. The system dynamic equations consist of the Earth's geo-potential, the atmospheric drag and the lunar/solar gravitational perturbations. The range, azimuth and elevation angles of the satellite measured from ground stations are used for orbit determination. The numerical results of the non-recursive unscented batch algorithm are compared with those of the well-known batch least squares estimation, the non-recursive Gaussian least squares estimation. The characteristics of the non-recursive unscented batch filter are analyzed for various aspects, including accuracy of the determined orbit, sensitivity to the initial uncertainty, measurement incompleteness and stability performance in a realistic dynamic system and measurement model.

## 2. Orbit determination

The orbit determination problem is to estimate accurately the ephemeris of an orbiting satellite at a chosen epoch. To achieve this goal, estimations of the state and the model parameters of the satellite are made based on a sequence of observations. The dynamic models of the equations of motion are usually integrated from a chosen epoch to each observation times to produce predicted observations. The differences between the predicted observations and true observations are defined as the observation residuals. Then, components of the state vector at a chosen epoch are corrected to minimize the observation residuals in a least squares sense. Thus, solving the orbit determination problem requires [9]: (i) equations of motion describing the forces acting on the satellite, (ii) the relationship between the observed parameters and the satellite's state vector, and (iii) an estimation algorithm. These steps used in the present paper are described in the next sections.

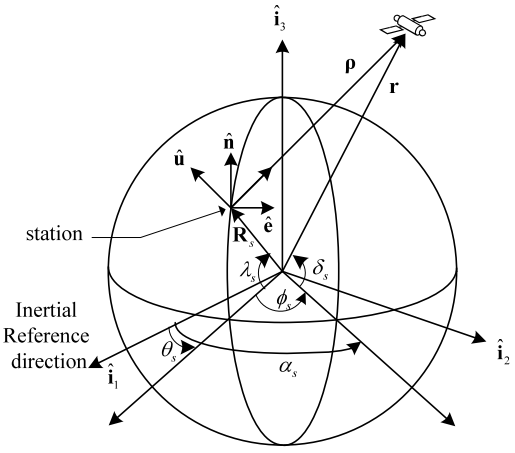


**Fig. 1.** Geometry of Earth observation of satellite motion [4].

### 2.1. Force models

The equations of motion of a satellite are usually described in an inertial reference frame as being composed of a sum of gravitational, non-gravitational and empirical or un-modeled forces. In the current research, the equations of motion for an Earth orbiting satellite are given by

$$\dot{\mathbf{r}} = \mathbf{v} \tag{1}$$

$$\dot{\mathbf{v}} = -\frac{\mu}{r^3}\mathbf{r} + \mathbf{a}_{perturbed} = \mathbf{a}_{geo} + \mathbf{a}_{Sun/Moon} + \mathbf{a}_{drag} \tag{2}$$

where $\mathbf{r}$ and $\mathbf{v}$ are the position and velocity vectors in the inertial frame [20]. The forces ($\dot{\mathbf{v}}$) acting on the satellite consist of the two-body effect and the addictive perturbing accelerations. $\mathbf{a}_{geo}$ is the geo-potential force due to the gravitational force of the Earth and can be expressed as a spherical harmonic expansion of the gradient of the Earth's solid body distribution. $\mathbf{a}_{Sun/Moon}$ is the lunar/solar gravitational perturbation, which are usually modeled as point masses within the Newtonian framework. $\mathbf{a}_{drag}$ is the atmospheric drag force described as follows,

$$\mathbf{a}_{drag} = -\frac{1}{2}\frac{C_D A}{M}\rho v_r \mathbf{v}_r \tag{3}$$

$$B^* = \frac{C_D A}{M} \tag{4}$$

The coefficient of drag, $C_D$, is a dimensionless quantity which reflects the satellite's susceptibility to drag force. The atmospheric density, $\rho$, indicates how dense the atmosphere is at the satellite's altitude. The cross-sectional area, $A$, is defined to be the area which is normal to the satellite's velocity vector. $\mathbf{v}_r$ is the velocity vector of the satellite relative to the atmosphere and $v_r$ is its norm. $B^*$ is the inverse of the ballistic coefficient of the satellite, defined by the multiplication of the coefficient of drag and the area-to-mass ratio ($A/M$). The JGM3 model for geo-potential coefficients [14] (a degree of $10\times10$), the analytical formulas for the lunar/solar ephemeris [14] and the Harris–Priester model [14] for the atmospheric density are used. All the equations of motion are numerically integrated by the Runge–Kutta fourth-order fixed step method.

### 2.2. Measurement model

We consider a ground tracking station that measures a range, azimuth and elevation of a satellite in orbit. The geometry asso-

ciated with this observation is shown in Fig. 1. In Fig. 1, $\boldsymbol{\rho}$ is the slant range vector, $\mathbf{r}$ is the radius vector locating the satellite, $\mathbf{R}_s$ is the radius vector locating the ground tracking station, $\alpha_s$ and $\delta_s$ are the right ascension and declination of the satellite, respectively, $\theta_s$ is the sidereal time of the ground station, $\lambda_s$ is the latitude of the ground tracking station, and $\phi_s$ is the east longitude from the ground tracking station to the satellite. The fundamental observation is given by

$$\boldsymbol{\rho} = \mathbf{r} - \mathbf{R}_s \tag{5}$$

In non-rotating equatorial components the vector $\boldsymbol{\rho}$ is given by [4]

$$\boldsymbol{\rho} = \begin{bmatrix} x - \|\mathbf{R}_s\| \cos\lambda_s \cos\theta_s \\ y - \|\mathbf{R}_s\| \cos\lambda_s \sin\theta_s \\ z - \|\mathbf{R}_s\| \sin\lambda_s \end{bmatrix} \tag{6}$$

where $x$, $y$, and $z$ are the components of the vector $\mathbf{r}$. The ground tracking station coordinate system (up, east and north) is described in Fig. 1. The conversion from the inertial to ground tracking station coordinate is given by [4]

$$\begin{bmatrix} \rho_u \\ \rho_e \\ \rho_n \end{bmatrix} = \begin{bmatrix} \cos\lambda_s & 0 & \sin\lambda_s \\ 0 & 1 & 0 \\ -\sin\lambda_s & 0 & \cos\lambda_s \end{bmatrix} \begin{bmatrix} \cos\theta_s & \sin\theta_s & 0 \\ -\sin\theta_s & \cos\theta_s & 0 \\ 0 & 0 & 1 \end{bmatrix} \boldsymbol{\rho} \tag{7}$$

A ground tracking station measures the azimuth (az), elevation (el), and range ($\rho$). The measurement equations are given by [4]

$$\rho = \sqrt{\rho_u^2 + \rho_e^2 + \rho_n^2} \tag{8}$$

$$\text{az} = \tan^{-1}\left(\frac{\rho_e}{\rho_n}\right) \tag{9}$$

$$\text{el} = \tan^{-1}\left(\frac{\rho_u}{\sqrt{\rho_n^2 + \rho_e^2}}\right) \tag{10}$$

Hence, the measurement data used in the present paper are azimuth (az), elevation (el) and range ($\rho$).

## 3. Estimation algorithms

In this section the batch least squares estimation algorithm is reviewed and the non-recursive unscented batch filter using the unscented transformation is proposed for orbit determination. The basic dynamic and measurement equations for describing estimation algorithms are as follows,

$$\mathbf{x}_{k+1} = \mathbf{f}(\mathbf{x}_k, \mathbf{w}_k, t_k) \tag{11}$$

$$\mathbf{y}_k = \mathbf{h}(\mathbf{x}_k, t_k) + \boldsymbol{\nu}_k \tag{12}$$

where $\mathbf{f}$ is the system function and it is associated with Eqs. (1)–(2). $\mathbf{h}$ is the measurement function and it is composed of Eqs. (8)–(10). $\mathbf{x}_k$ is the state vector at time $t_k$ with a covariance of $\mathbf{P}_k$, and $\mathbf{y}_k$ is the measurement vector. $\mathbf{w}_k$ and $\boldsymbol{\nu}_k$ are the process noise vector and the addictive measurement noise vector, respectively, which have a zero-mean Gaussian distribution with covariance of $\mathbf{Q}_k$ and $\mathbf{R}_k$, respectively. In addition, $\mathbf{w}_k$ and $\boldsymbol{\nu}_k$ are uncorrelated.

### 3.1. The batch least squares estimation

The batch least squares filter selects the estimate of state at a chosen epoch as the value that minimizes the sum of the squares of measurement residuals, and it is processed using an entire set of measurements. So, the measurement function, Eq. (12), is redefined by

$$\tilde{\mathbf{y}}_k \equiv \begin{bmatrix} \mathbf{y}_1 \\ \mathbf{y}_2 \\ \vdots \\ \mathbf{y}_N \end{bmatrix} \equiv \begin{bmatrix} \mathbf{h}(\mathbf{x}_1) \\ \mathbf{h}(\mathbf{x}_2) \\ \vdots \\ \mathbf{h}(\mathbf{x}_N) \end{bmatrix} + \begin{bmatrix} \boldsymbol{\nu}_1 \\ \boldsymbol{\nu}_2 \\ \vdots \\ \boldsymbol{\nu}_N \end{bmatrix} \equiv \tilde{\mathbf{h}}(\mathbf{x}_k) + \tilde{\boldsymbol{\nu}}_k \tag{13}$$

where the subscript notes a chosen epoch $t_k$ ($t_1 \leqslant t_k \leqslant t_N$), $N$ is the number of measurement epochs, the tilde symbols of $\tilde{\mathbf{y}}_k$ and $\tilde{\boldsymbol{\nu}}_k$ relate to the entire set of each measurement and measurement noise, respectively, and $\tilde{\mathbf{h}}$ is the mapping matrix which is expressed in terms of the state at a chosen epoch $t_k$.

For the orbit determination problem, the practical solution of the batch least squares is complicated by the fact that $\tilde{\mathbf{h}}$, in Eq. (13), is a highly nonlinear function of the state $\mathbf{x}_k$, which makes it difficult or impossible to get an exact solution [14]. So, by assuming a reference orbit is sufficiently close to the unknown true orbit, in other words, the deviation or difference ($\Delta\mathbf{x}_k$) of the two trajectories is small, the dynamics of the unknown true orbit is linearized about the assumed reference orbit and given by

$$\Delta\dot{\mathbf{x}}_k = \mathbf{F}_k \Delta\mathbf{x}_k \tag{14}$$

where $\mathbf{F}_k$ is the partial derivative of $\mathbf{f}$ with respect to the state vector, and Eq. (13) can be linearized as follows,

$$\Delta\tilde{\mathbf{y}}_k = \tilde{\mathbf{H}}_k \Delta\mathbf{x}_k + \tilde{\boldsymbol{\nu}}_k \tag{15}$$

where $\tilde{\mathbf{H}}_k$ is the partial derivative of $\tilde{\mathbf{h}}$ with respect to the state vector.

Then, the nonlinear orbit determination problem can be transformed to the linear problem about the state deviation ($\Delta\mathbf{x}$). When we wish to estimate the state deviation vector $\Delta\mathbf{x}_k$ at reference time, $t_k$, the best estimate value ($\Delta\hat{\mathbf{x}}_k$) of state is expressed by the normal equation as follows [19],

$$\Delta\hat{\mathbf{x}}_k = \left(\tilde{\mathbf{H}}_k^T \tilde{\mathbf{R}}_k^{-1} \tilde{\mathbf{H}}_k + \bar{\mathbf{P}}_k^{-1}\right)^{-1} \left(\tilde{\mathbf{H}}_k^T \tilde{\mathbf{R}}_k^{-1} \Delta\tilde{\mathbf{z}}_k + \bar{\mathbf{P}}_k^{-1} \Delta\bar{\mathbf{x}}_k\right) \tag{16}$$

$$\hat{\mathbf{P}}_k = \left(\tilde{\mathbf{H}}_k^T \tilde{\mathbf{R}}_k^{-1} \tilde{\mathbf{H}}_k + \bar{\mathbf{P}}_k^{-1}\right)^{-1} \tag{17}$$

where $\Delta\bar{\mathbf{x}}_k$ and $\bar{\mathbf{P}}_k$ are a priori calculations of state and covariance at epoch time $t_k$, and $\Delta\hat{\mathbf{x}}_k$ and $\hat{\mathbf{P}}_k$ are the estimated differential correction of the state and covariance at the epoch time. The measurement residual, $\Delta\tilde{\mathbf{z}}_k$, is the difference between the actual measurement and calculated measurement using numerical models. $\tilde{\mathbf{R}}_k$ is the measurement noise covariance. The subscript $k$ means that all of the measurement residuals are calculated using the state at chosen epoch time, $t_k$. The right side of Eqs. (16)–(17) can be calculated by [19]

$$\tilde{\mathbf{H}}_k^T \tilde{\mathbf{R}}_k^{-1} \tilde{\mathbf{H}}_k = \sum_{i=1}^{N} (\mathbf{H}_i \boldsymbol{\Phi}_{i,k})^T \mathbf{R}_i^{-1} (\mathbf{H}_i \boldsymbol{\Phi}_{i,k}) \tag{18}$$

$$\tilde{\mathbf{H}}_k^T \tilde{\mathbf{R}}_k^{-1} \Delta\tilde{\mathbf{z}}_k = \sum_{i=1}^{N} (\mathbf{H}_i \boldsymbol{\Phi}_{i,k})^T \mathbf{R}_i^{-1} \Delta\mathbf{z}_i \tag{19}$$

where $\mathbf{H}_i$ is the partial derivative of $\tilde{\mathbf{h}}$ with respect to the state vector at time $t_i$, $\boldsymbol{\Phi}_{i,k}$ is the state transition matrix from $\mathbf{x}_k$ to $\mathbf{x}_i$, $\Delta\mathbf{z}_i$ is the measurement residual at time $t_i$, and $\mathbf{R}_i$ is the measurement noise covariance at time $t_i$. Because the orbit determination problem is not linear, the state of the initial guess is updated by iteration. Hence, there must be a standard value to quit the estimation process. The root mean square (RMS) value of the measurement residual is commonly used to determine the convergence criterion [20], $\varepsilon$.

$$\text{RMS}_{new} = \left\{ \frac{\sum_{i=1}^{N} \Delta\tilde{\mathbf{z}}_i^T \tilde{\mathbf{R}}_i^{-1} \Delta\tilde{\mathbf{z}}_i}{n_{meas}(N)} \right\}, \quad \left| \frac{\text{RMS}_{new} - \text{RMS}_{old}}{\text{RMS}_{old}} \right| < \varepsilon \tag{20}$$

where $n_{meas}$ is the number of different types of measurements.

In this subsection, the batch least square estimation process is summarized. The main characteristic of the batch least squares filter is the linearization approximation of nonlinear equations. The nonlinear system, Eq. (11), and measurement equations, Eq. (13), are linearized and approximated by Taylor's series expansion with excluding high order terms. Then the linear equations, Eqs. (14)–(15), are derived. The linearized equations include the partial derivatives of system and measurement equations with respect to the state. So, when the complexities of the nonlinear equations and the number of state are increasing, the partial derivative calculations are severely complicated.

### 3.2. Unscented transformation and non-recursive unscented batch filter

In this section, the conventional unscented Kalman filter (UKF) algorithm is reviewed and the non-recursive unscented batch filter algorithm using the unscented transformation is introduced. Because both the filters are all based on the unscented transformation, the non-recursive unscented batch filter can be explained from the UKF algorithm. So, the basic UKF process is reviewed briefly. The basic functions of the system and measurement from Eqs. (11)–(12) are used for describing algorithms in this section.

The most important feature of the UKF is computing the mean and the covariance of nonlinearly transformed variables from some selected variables (sigma points) without a traditional linear approximation of the nonlinear function [10]. Therefore, the UKF can calculate the mean and covariance more accurately than the extended Kalman filter (EKF) method which uses a linear approximation of the nonlinear system. The UKF process starts with the selection of sigma points, which are the set of points around the original reference state vector. It is redefined as an augmented state vector ($\mathbf{x}_k^a$) along with noise variables, and the augmented covariance matrix ($\mathbf{P}_k^a$) on the diagonal is reconstructed by [21]

$$\mathbf{x}_k^a = \begin{bmatrix} \mathbf{x}_k \\ \mathbf{w}_k \end{bmatrix}, \qquad \mathbf{P}_k^a = \begin{bmatrix} \mathbf{P}_k & 0 \\ 0 & \mathbf{Q}_k \end{bmatrix} \tag{21}$$

Assuming the initial state and its covariance as $\hat{\mathbf{x}}_k^a$ $(= [\mathbf{x}_k^T, 0]^T)$ and $\hat{\mathbf{P}}_k^a$, respectively, the set of scaled symmetric sigma points with the augmented state vector and covariance matrix are constructed by [21]

$$\begin{aligned} \hat{\boldsymbol{\chi}}_{0,k}^{\,a} &= \hat{\mathbf{x}}_k^a \\ \hat{\boldsymbol{\chi}}_{i,k}^{\,a} &= \hat{\mathbf{x}}_k^a + \Big(\sqrt{(L+\lambda)\hat{\mathbf{P}}_k^a}\Big)_i, \quad i = 1, \ldots, L \\ \hat{\boldsymbol{\chi}}_{i,k}^{\,a} &= \hat{\mathbf{x}}_k^a - \Big(\sqrt{(L+\lambda)\hat{\mathbf{P}}_k^a}\Big)_{i-L}, \quad i = L+1, \ldots, 2L \end{aligned} \tag{22}$$

where $\hat{\boldsymbol{\chi}}_k^{\,a}$ represents the augmented state vector consisting of state $\hat{\boldsymbol{\chi}}_k^{\,x}$ and process noise $\hat{\boldsymbol{\chi}}_k^{\,w}$, $L$ is the dimension of the augmented state, and $\lambda$ $(\equiv \alpha^2(L+\kappa) - L)$ is the scaling parameter. The constant $\alpha$ decides the extent of the sigma points, and is usually set to a small positive value. The secondary scaling parameter $\kappa$ is generally set to $3 - L$. $(\sqrt{(L+\lambda)\hat{\mathbf{P}}_k^a})_i$ means the $i$th column of the matrix square root of the augmented covariance ($\hat{\mathbf{P}}_k^a$). The total number of sigma points is $(2L+1)$. Each sigma point is propagated to the next measurement time ($t_{k+1}$) using the nonlinear function $\mathbf{f}$ from Eq. (11) as follows,

$$\bar{\boldsymbol{\chi}}_{i,k+1}^{\,a} = \mathbf{f}\big(\hat{\boldsymbol{\chi}}_{i,k}^{\,x}, \hat{\boldsymbol{\chi}}_{i,k}^{\,w}, t_k\big), \quad i = 1, \ldots, 2L \tag{23}$$

The measurement vector ($\boldsymbol{\gamma}_{i,k+1}$) at each propagated sigma point ($\bar{\boldsymbol{\chi}}_{i,k+1}^{\,x}$) is also calculated thorough the nonlinear function $\mathbf{h}$ from Eq. (12) as follows,

$$\boldsymbol{\gamma}_{i,k+1} = \mathbf{h}\big(\bar{\boldsymbol{\chi}}_{i,k+1}^{\,x}, t_{k+1}\big) \tag{24}$$

If the measurement noise is addictive, the augmented state vector will be defined by adding only the process noise to the state vector. This helps the computational speed because of the decrease of the number of sigma points. The predicted state ($\bar{\mathbf{x}}_{k+1}$) and measurement vector ($\bar{\mathbf{y}}_{k+1}$) and their covariances ($\bar{\mathbf{P}}_{k+1}, \bar{\mathbf{P}}_{k+1}^{y}$) are calculated as a form of the weighted mean of the propagated sigma points ($\bar{\boldsymbol{\chi}}_{i,k+1}^{\,x}$) and the measurement vector ($\boldsymbol{\gamma}_{i,k+1}$) through the nonlinear functions as follows [21]:

For state,

$$\bar{\mathbf{x}}_{k+1} = \sum_{i=0}^{2L} W_i^{(m)} \bar{\boldsymbol{\chi}}_{i,k+1}^{\,x}, \quad i = 1, \ldots, 2L \tag{25}$$

$$\bar{\mathbf{P}}_{k+1} = \sum_{i=0}^{2L} W_i^{(c)} \big(\bar{\boldsymbol{\chi}}_{i,k+1}^{\,x} - \bar{\mathbf{x}}_{k+1}\big)\big(\bar{\boldsymbol{\chi}}_{i,k+1}^{\,x} - \bar{\mathbf{x}}_{k+1}\big)^T \tag{26}$$

For measurement,

$$\bar{\mathbf{y}}_{k+1} = \sum_{i=0}^{2L} W_i^{(m)} \boldsymbol{\gamma}_{i,k+1} \tag{27}$$

$$\bar{\mathbf{P}}_{k+1}^{y} = \sum_{i=0}^{2L} W_i^{(c)} (\boldsymbol{\gamma}_{i,k+1} - \bar{\mathbf{y}}_{k+1})(\boldsymbol{\gamma}_{i,k+1} - \bar{\mathbf{y}}_{k+1})^T + \mathbf{R}_{k+1} \tag{28}$$

and the cross-correlation matrix ($\bar{\mathbf{P}}^{xy}$) of $\mathbf{x}, \mathbf{y}$ is computed by

$$\bar{\mathbf{P}}_{k+1}^{xy} = \sum_{i=0}^{2L} W_i^{(c)} \big(\bar{\boldsymbol{\chi}}_{i,k+1}^{\,x} - \bar{\mathbf{x}}_{k+1}\big)(\boldsymbol{\gamma}_{i,k+1} - \bar{\mathbf{y}}_{k+1})^T \tag{29}$$

where the weighing factors ($W_i^{(m)}, W_i^{(c)}$) for the state and covariance are computed as follows,

$$W_i^{(m)} = \begin{cases} \frac{\lambda}{(L+\lambda)}, & i = 0 \\ \frac{1}{2(L+\lambda)}, & i = 1, \ldots, 2L \end{cases} \tag{30}$$

$$W_i^{(c)} = \begin{cases} \frac{\lambda}{(L+\lambda)} + 1 - \alpha^2 + \beta, & i = 0 \\ \frac{1}{2(L+\lambda)}, & i = 1, \ldots, 2L \end{cases} \tag{31}$$

The third scaling parameter $\beta$ plays a role in incorporating prior knowledge of the distribution of $\mathbf{x}$, and $\beta = 2$ is known to be optimal for the Gaussian distribution. The corrected state ($\hat{\mathbf{x}}_{k+1}$) and covariance ($\hat{\mathbf{P}}_{k+1}$) of the UKF have the same formulas as the standard Kalman filter, namely [21],

$$\hat{\mathbf{x}}_{k+1} = \bar{\mathbf{x}}_{k+1} + \mathbf{K}_{k+1}(\tilde{\mathbf{y}}_{k+1} - \bar{\mathbf{y}}_{k+1}) \tag{32}$$

$$\hat{\mathbf{P}}_{k+1} = \bar{\mathbf{P}}_{k+1} - \mathbf{K}_{k+1}\bar{\mathbf{P}}_{k+1}^{xy}\mathbf{K}_{k+1}^T \tag{33}$$

where $\tilde{\mathbf{y}}_{k+1}$ is the observed measurement vector, and the gain matrix $\mathbf{K}_{k+1}$ is defined by

$$\mathbf{K}_{k+1} = \bar{\mathbf{P}}_{k+1}^{xy}\big(\bar{\mathbf{P}}_{k+1}^{y}\big)^{-1} \tag{34}$$

Assuming an observation is composed of $n_{meas}$ different types of measurements, the dimensions of the measurement matrix ($\bar{\mathbf{y}}_k$) and covariance matrix ($\bar{\mathbf{P}}_k^y$) in Eqs. (27)–(28) are $n_{meas} \times 1$ and $n_{meas} \times n_{meas}$, respectively. In Eqs. (29) and (34), the dimensions of the cross-correlation matrix ($\bar{\mathbf{P}}_k^{xy}$) and gain matrix ($\mathbf{K}_k$) are the same as $L \times n_{meas}$. A batch formulation provides an estimate of the state at a chosen epoch using a set of measurement data. The sequential processor, on the other hand, provides an estimate of the state at each measurement time based on observations up to that time. Although there are distinct differences in both the methods, there are also similarities between the two methods. In sequential formulation without process noise, a mathematical equivalence can be shown between batch and sequential algorithms [19]; given

the same measurement data set, both the algorithms produce the same estimates when the estimates are mapped to the same times. In the extended form of the sequential algorithm, where the reference orbit is updated at each measurement time, the algorithms are not equivalent, but numerical experiments have shown a very close agreement [19]. Hence, the conventional UKF formulations are very helpful to construct the non-recursive unscented batch filter developed in the current study.

The non-recursive unscented batch filter for orbit determination is proposed as follows. Ordinarily, the process noise is not considered in the batch process [6] because the batch process obtains convergence by iterations without the process noise compensation. In addition, the process noise makes the calculation slower and complicated due to the increase of the dimensions of the normal matrix. Additionally, if the measurement noise is assumed to be addictive, the algorithm can be derived from a non-augmented UKF. So, Eq. (21) is expressed by

$$\mathbf{x}_k^a = \mathbf{x}_k, \qquad \mathbf{P}_k^a = \mathbf{P}_k \tag{35}$$

Firstly, the initial state estimate and its covariance estimate are assumed by

$$\hat{\mathbf{x}}_k = \hat{\mathbf{x}}_{initial}, \qquad \hat{\mathbf{P}}_k = \hat{\mathbf{P}}_{initial} \tag{36}$$

where $k$ means the epoch time $t_k$ (to be estimated) and the sigma points are selected by

$$\begin{aligned}
&\hat{\boldsymbol{\chi}}_{0,k} = \hat{\mathbf{x}}_k \\
&\hat{\boldsymbol{\chi}}_{i,k} = \hat{\mathbf{x}}_k + \left(\sqrt{(L+\lambda)\hat{\mathbf{P}}_k}\right)_i, \quad i = 1, \ldots, L \\
&\hat{\boldsymbol{\chi}}_{i,k} = \hat{\mathbf{x}}_k - \left(\sqrt{(L+\lambda)\hat{\mathbf{P}}_k}\right)_{i-L}, \quad i = L+1, \ldots, 2L
\end{aligned} \tag{37}$$

The UKF recursively updates the state vector to produce a better estimate at each epoch, so the state is propagated to the next measurement time using Eq. (23). However, the non-recursive unscented batch filter estimates a chosen epoch using all the measurement set of data. So, the propagations of sigma points at a chosen epoch are equal to the previously estimated values, and the propagated state and associated covariance at the chosen epoch can be directly set as follows [8] without calculating Eqs. (23), (25), and (26),

$$\bar{\boldsymbol{\chi}}_{i,k} = \hat{\boldsymbol{\chi}}_{i,k}, \qquad \bar{\mathbf{x}}_k = \hat{\mathbf{x}}_k, \qquad \bar{\mathbf{P}}_k = \widehat{\mathbf{P}}_k, \quad i = 0, \ldots, 2L \tag{38}$$

Selected sigma points $\bar{\boldsymbol{\chi}}_{i,k}$ $(i = 0, \ldots, 2L)$ at a chosen epoch are propagated for calculating all the measurement data set. Each sigma point is propagated and the measurement vectors are calculated to each measurement time $(t_j, j = 1, \ldots, N, j \neq k)$ by using the nonlinear function $\mathbf{h}$ from Eq. (12) as follows [8],

$$\tilde{\boldsymbol{\gamma}}_{i,k} = \tilde{\mathbf{h}}(\bar{\boldsymbol{\chi}}_{i,k}) = \begin{bmatrix} \boldsymbol{\gamma}_{i,1} \\ \boldsymbol{\gamma}_{i,2} \\ \vdots \\ \boldsymbol{\gamma}_{i,N} \end{bmatrix} = \begin{bmatrix} \mathbf{h}(\bar{\boldsymbol{\chi}}_{i,1}, t_1) \\ \mathbf{h}(\bar{\boldsymbol{\chi}}_{i,2}, t_2) \\ \vdots \\ \mathbf{h}(\bar{\boldsymbol{\chi}}_{i,N}, t_N) \end{bmatrix}, \quad i = 0, \ldots, 2L \tag{39}$$

where $\bar{\boldsymbol{\chi}}_{i,j}$ (i.e. $\bar{\boldsymbol{\chi}}_{i,1}, \bar{\boldsymbol{\chi}}_{i,2}, \ldots, \bar{\boldsymbol{\chi}}_{i,N}$) on the right side of Eq. (39) are the propagated sigma points for each measurement time $(t_j, j = 1, \ldots, N, j \neq k)$ and $N$ is the total number of measurement times.

The propagated measurements and covariances at each measurement time are calculated by

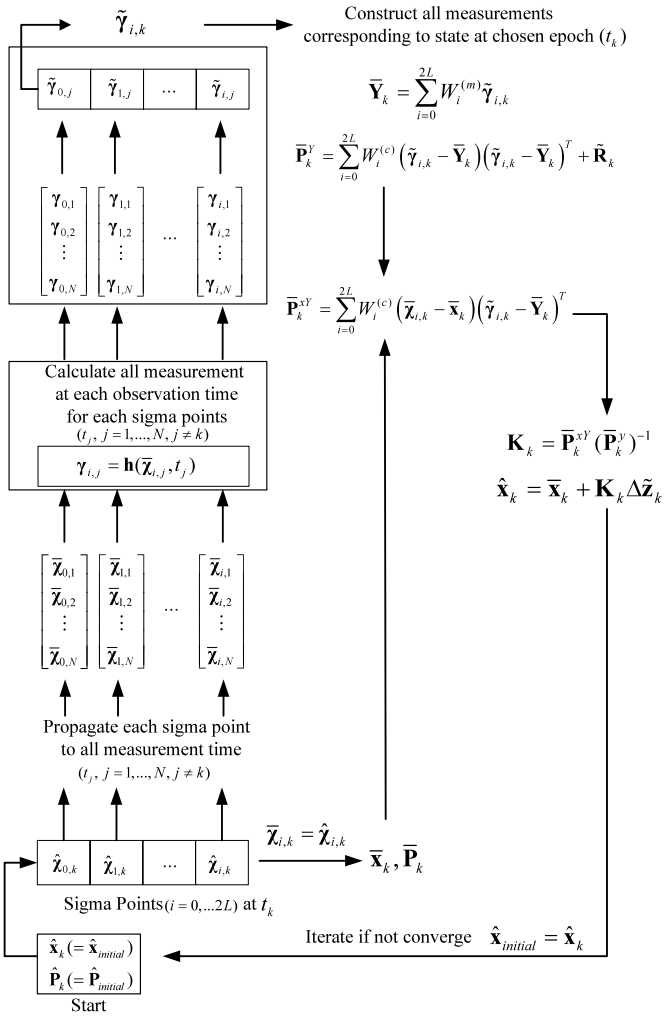


**Fig. 2.** Flow of the non-recursive unscented batch filter.

$$\bar{\mathbf{Y}}_k = \begin{bmatrix} \bar{\mathbf{y}}_1 \\ \bar{\mathbf{y}}_2 \\ \vdots \\ \bar{\mathbf{y}}_N \end{bmatrix} = \sum_{i=0}^{2L} W_i^{(m)} \tilde{\boldsymbol{\gamma}}_{i,k} \tag{40}$$

$$\bar{\mathbf{P}}_k^Y = \sum_{i=0}^{2L} W_i^{(c)} (\tilde{\boldsymbol{\gamma}}_{i,k} - \bar{\mathbf{Y}}_k)(\tilde{\boldsymbol{\gamma}}_{i,k} - \bar{\mathbf{Y}}_k)^T + \tilde{\mathbf{R}}_k \tag{41}$$

where $\tilde{\mathbf{R}}_k$ is the measurement noise matrix and the cross-correlation matrix is computed by

$$\bar{\mathbf{P}}_k^{xY} = \sum_{i=0}^{2L} W_i^{(c)} (\bar{\boldsymbol{\chi}}_{i,k} - \bar{\mathbf{x}}_k)(\tilde{\boldsymbol{\gamma}}_{i,k} - \bar{\mathbf{Y}}_k)^T \tag{42}$$

And the gain matrix is defined by

$$\mathbf{K}_k = \bar{\mathbf{P}}_k^{xY} \left(\bar{\mathbf{P}}_k^Y\right)^{-1} \tag{43}$$

Finally, the state at epoch time $t_k$ is updated by

$$\hat{\mathbf{x}}_k = \bar{\mathbf{x}}_k + \mathbf{K}_k(\tilde{\mathbf{Y}}_k - \bar{\mathbf{Y}}_k) = \bar{\mathbf{x}}_k + \mathbf{K}_k \Delta\tilde{\mathbf{z}}_k \tag{44}$$

where $\Delta\tilde{\mathbf{z}}_k$ is the measurement residual matrix calculated by the difference between the actual $(\tilde{\mathbf{Y}}_k)$ and computed $(\bar{\mathbf{Y}}_k)$ measurement of all measurement times.

The non-recursive unscented batch filter algorithms from Eqs. (40)–(44) are described in the similar forms to the UKF (Eqs. (25)–(34)) for convenience. But, there are lots of differences. If

the number of different types of measurements is $n_{meas}$, the total number ($N_{tot}$) of measurement data is equal to $n_{meas} \times N$. The dimensions of the measurement matrix ($\bar{\mathbf{Y}}_k$) and covariance matrix ($\bar{\mathbf{P}}_k^Y$) in Eqs. (40)–(41) are $N_{tot} \times 1$ and $N_{tot} \times N_{tot}$, respectively. In Eqs. (42)–(43), the dimensions of the cross-correlation matrix ($\bar{\mathbf{P}}_k^{xY}$) and gain matrix ($\mathbf{K}_k$) are the same as $L \times N_{tot}$. The initial state from Eq. (36) is corrected and updated using Eq. (44) iteratively. The iterations are terminated by the same condition of the batch least squares filter in Eq. (20). The proposed algorithm estimates system states and parameters at a chosen epoch time (not successive time) by using the measurements collected over a fixed time span at a time. This is the main difference from iterative or smoother filters which process measurements sequentially in forward or backward directions. In Fig. 2, the non-recursive unscented batch filter process is summarized as a flowchart. The initial covariance is reset after iteration since there is no propagation of covariance and new information for additional measurement data.

## 4. Numerical simulations and results

Numerical simulations are carried out to demonstrate the performance of the non-recursive unscented batch filter in orbit determination problems. The performance of the non-recursive unscented batch filter is also compared with that of the existing batch least squares filter in various aspects, using realistic dynamic and measurement models for a low-Earth orbiting satellite. The basic configurations, test cases, and results for the numerical simulations are described in the following subsections.

### 4.1. Measurement data simulations and initial configurations

In this study, the true orbit ephemeris and measurement data are assumed to be generated by the High Precision Orbit Propagator (HPOP) in the Satellite Tool Kit (STK) [18,22] for orbit determination. In the HPOP module, the Gauss–Jackson method for the numerical integration of the equations of motion, the EGM 96 model (up to a degree of $70 \times 70$) for perturbation due to the non-symmetric geo-potential, the Jacciha70 model for the atmospheric density, and the DE403 JPL coefficient for the lunar/solar ephemeris are used. Atmospheric drag, lunar/solar gravitational attraction, and solar radiation pressure are also included. The atmospheric drag coefficient is set to 2.0, the solar radiation pressure coefficient is set to 1.0, and the constant area-to-mass ratio is set to 0.02 $m^2/kg$. For the equations of motion of the orbit determination system (described in Section 2), some model parameters are set differently as follows: The atmospheric drag coefficient is set to 2.3, the solar radiation pressure coefficient is set to 1.2, and the constant area-to-mass ratio is set to 0.022 $m^2/kg$. By using different dynamic models for measurement data simulation and orbit determination process, differences between the effects of the true perturbations (from the HPOP module) and those of the mathematically modeled perturbations (from dynamic models described in Section 2) can be considered. Hence, this approach may be more realistic for testing. The orbit calculated from the HPOP is considered as a true orbit, and is also used for verifying the accuracy of the orbit determination. The initial true osculating orbital elements at epoch time consist of the semi-major axis of 6778.14 km, the eccentricity of $10^{-5}$, the inclination of 51.60°, the right ascension of the ascending node of 25°, the argument of perigee of 30.046°, and the true anomaly of 359.95°. The observation data measured from three ground tracking stations are simulated for the low-Earth orbiting satellites for 12 hours from the epoch. The locations of the three selected stations are assumed as follows: Station 1 (geodetic longitude 30.23°, geodetic latitude 86.23°, height 0.04 km), Station 2 (geodetic longitude −30.00°, geodetic latitude −70.00°, height 0.10 km), and Station 3 (geodetic longitude 36.62°, geodetic latitude 139.82°, height 0.05 km). Each measurement data set is made up of range, azimuth, and elevation angles, which are calculated using the geometrical relationship between the satellite and ground tracking stations (described in Section 2). The measurement noises for each ground tracking station are modeled as a white Gaussian distribution. The measurement data are assumed to be obtained at the data-sampling period of 30 s from January 1, 2000, 12:00:00.0 (UTC) for 12 hours. The satellite can be accessed from the three ground tracking stations for a total of 17 times. The access times are indicated in Fig. 3. The cumulative dwell time is about 20% (2.5 hours) for the whole 12 hours. In other words, the measurement data from 17 tracks are sparse and separated. For all the numerical simulations, the position, $\mathbf{r}$, velocity, $\mathbf{v}$, and the inverse of the ballistic coefficient of the satellite, $B^*$, are considered as the components of the state vector $\mathbf{x} = [x, y, z, \dot{x}, \dot{y}, \dot{z}, B^*]$. For the scaled unscented transformation, the scaling parameter $\alpha$ is set to $10^{-3}$, and $\beta$ is set to 2, respectively. Because the process noises are not considered, the dimension of state, $L$, is set to 7 and the second scaling parameter $\kappa$ ($\equiv 3 - L$) is set to $-4$. So, $\lambda$ ($\equiv \alpha^2(L + \kappa) - L$) in Eq. (37) is equal to $-4 \times 10^{-6}$.

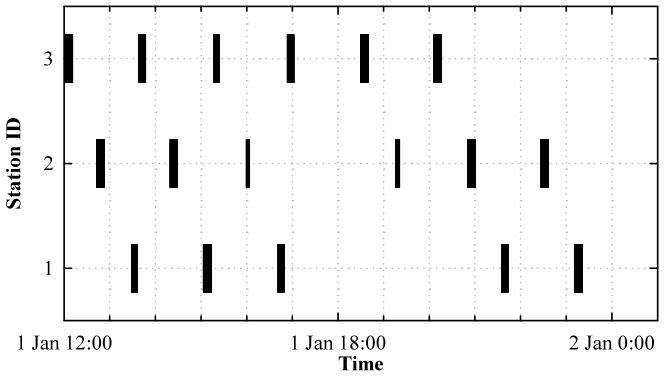


**Fig. 3.** Access times strip chart between the three ground tracking stations and Earth orbiting satellite assumed in the current study.

The states at a chosen epoch are determined using the batch least squares filter and the proposed filter. From the estimated states at a chosen epoch, the orbit ephemeris data are generated from a specified epoch to a final time (for 12 hours) and compared with the reference orbit calculated by HPOP. The RMS differences between the generated orbit and reference orbit in radial, along track, cross track, and position are applied for the performance assessment of both the filters. Because the batch algorithms are used in an iterative fashion, the absolute magnitudes of position errors at a chosen epoch for each iteration, the number of iterations, and computing time for the filter convergence are also considered as the performance criteria. For all simulation tests, the estimation convergence criterion in Eq. (20) is set to $10^{-3}$.

### 4.2. Effects of the initial errors in position and velocity

In this subsection, effects of the initial errors in position and velocity are tested and compared in six cases for the two estimation algorithms, the non-recursive unscented batch filter and the batch least squares filter. The initial errors in position and velocity are assumed to be added [1 km, 1 km, 1 km, 1 m/s, 1 m/s, 1 m/s] for Case-1, [5 km, 5 km, 5 km, 5 m/s, 5 m/s, 5 m/s] for Case-2, [10 km, 10 km, 10 km, 10 m/s, 10 m/s, 10 m/s] for Case-3, [15 km, 15 km, 15 km, 15 m/s, 15 m/s, 15 m/s] for Case-4, [20 km, 20 km, 20 km, 20 m/s, 20 m/s, 20 m/s] for Case-5, and [30 km, 30 km, 30 km, 30 m/s, 30 m/s, 30 m/s] for Case-6, and for each component of the true initial position and velocity vectors are $\mathbf{r}_0^{true} = [4430.3587 \text{ km}, 4388.6215 \text{ km}, 2655.9643 \text{ km}]$ and $\mathbf{v}_0^{true} = [-5.2185 \text{ km/s}, 2.1182 \text{ km/s}, 5.2047 \text{ km/s}]$. The initial

**Table 1**
RMS errors of radial, along track, cross track, and position for the non-recursive unscented batch filter with various initial errors in position and velocity.

| Case | Radial error (m, RMS) | Along error (m, RMS) | Cross error (m, RMS) | Position error (m, RMS) | Iteration # | Computing time (s) |
|---|---|---|---|---|---|---|
| 1 | 9.84 | 26.64 | 8.87 | 29.76 | 6 | 138 |
| 2 | 9.84 | 26.64 | 8.88 | 29.75 | 6 | 121 |
| 3 | 9.84 | 26.64 | 8.88 | 29.76 | 7 | 159 |
| 4 | 9.84 | 26.63 | 8.88 | 29.75 | 7 | 176 |
| 5 | 9.84 | 26.60 | 8.87 | 29.72 | 8 | 189 |
| 6 | 9.87 | 26.74 | 8.89 | 29.86 | 9 | 212 |

**Table 2**
RMS errors of radial, along track, cross track, and position for the batch least squares filter with various initial errors in position and velocity.

| Case | Radial error (m, RMS) | Along error (m, RMS) | Cross error (m, RMS) | Position error (m, RMS) | Iteration # | Computing time (s) |
|---|---|---|---|---|---|---|
| 1 | 10.48 | 27.42 | 8.87 | 30.66 | 8 | 57 |
| 2 | 10.50 | 27.42 | 8.86 | 30.67 | 11 | 83 |
| 3 | 10.47 | 27.41 | 8.87 | 30.65 | 17 | 118 |
| 4 | 10.45 | 27.38 | 8.85 | 30.61 | 14 | 96 |
| 5 | N/A | N/A | N/A | N/A | N/A | N/A |
| 6 | N/A | N/A | N/A | N/A | N/A | N/A |

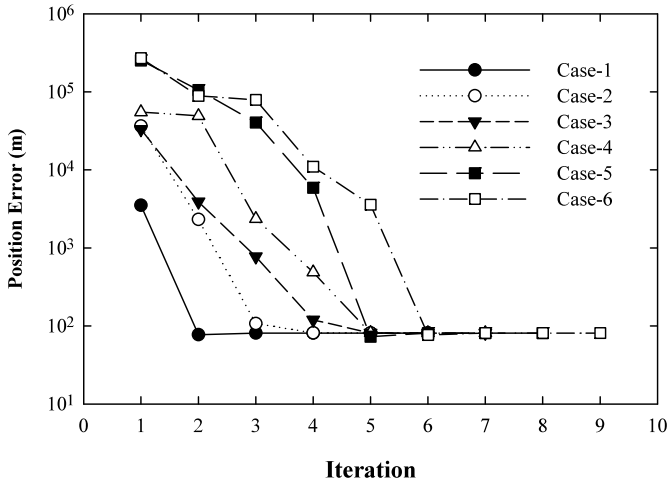

(a) non-recursive unscented batch filter

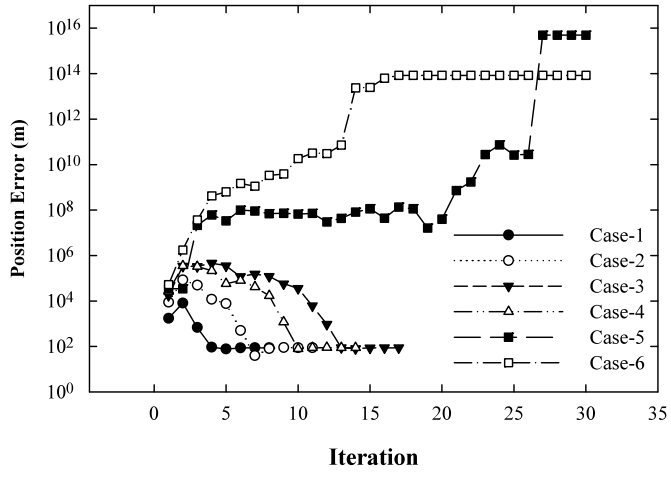

(b) batch least squares filter

**Fig. 4.** Histories of iterations and initial estimate errors in position for filters with various initial errors in position and velocity.

value of $B^*$ is assumed to be 0.05 for all six cases. The initial covariance matrix, $\mathbf{P}_0$, has diagonal components with position, velocity and $B^*$ elements. The initial covariance values of position and velocity errors for the six cases are set to [(100 m)$^2$, (100 m)$^2$, (100 m)$^2$, (0.1 m/s)$^2$, (0.1 m/s)$^2$, (0.1 m/s)$^2$] for Case-1, [(500 m)$^2$, (500 m)$^2$, (500 m)$^2$, (0.5 m/s)$^2$, (0.5 m/s)$^2$, (0.5 m/s)$^2$] for Case-2, [(1000 m)$^2$, (1000 m)$^2$, (1000 m)$^2$, (1 m/s)$^2$, (1 m/s)$^2$, (1 m/s)$^2$] for Case-3, [(1500 m)$^2$, (1500 m)$^2$, (1500 m)$^2$, (1.5 m/s)$^2$, (1.5 m/s)$^2$, (1.5 m/s)$^2$] for Case-4, [(2000 m)$^2$, (2000 m)$^2$, (2000 m)$^2$, (2 m/s)$^2$, (2 m/s)$^2$, (2 m/s)$^2$] for Case-5, and [(3000 m)$^2$, (3000 m)$^2$, (3000 m)$^2$, (3 m/s)$^2$, (3 m/s)$^2$, (3 m/s)$^2$] for Case-6. The initial covariance of $B^*$ is assumed to be $(0.005)^2$ for all six cases. The measurement data sampling period is assumed to be 30 s.

Figs. 4(a) and 4(b) describe the histories of iterations and the variations of the position errors with initial estimates at a chosen epoch time. The variation of the initial estimate errors indicates a filter correction by iteration. When the absolute magnitude of the initial estimate errors in position settle down and become stable after certain iterations, using the estimated initial state at the final iteration, the orbit ephemeris is generated for 12 hours and compared with that of the reference orbit. The RMS errors in radial, along track, cross track and position for 12 hours, iteration number, and computing time for the non-recursive unscented batch and the batch least squares estimations for various initial errors in position and velocity, are summarized in Table 1 and Table 2, respectively. For Case-1 to Case-4, both the filters are converged and yield similar accuracy in determined states. The RMS errors in position by the non-recursive unscented batch filter are slightly smaller than those by the batch least squares filter. As the initial errors in position and velocity are larger, the iteration and computing times are remarkably increased in the batch least squares filter. For Case-5 and Case-6, the batch least squares filter fails to converge, while the non-recursive unscented batch filter shows better convergence reliability. From these results, better robustness and efficiency are obtained by the non-recursive unscented batch process. For the batch least squares filter, the linearization process is executed with an assumption that the difference between the true orbit and the reference orbit are sufficiently small. Then, the large initial errors in position and velocity can cause a difficulty in convergence and in accurate estimation due to the nonlinearity problem. Hence, it can be concluded that the non-recursive unscented batch filter shows better convergence reliability if the nonlinearity of a system is strengthened.

**Table 3**
RMS errors of radial, along track, cross track, and position for the non-recursive unscented batch filter with various sampling periods.

| Sampling period (s) | Radial error (m, RMS) | Along error (m, RMS) | Cross error (m, RMS) | Position error (m, RMS) | Iteration # | Computing time (s) |
|---|---|---|---|---|---|---|
| 30 | 9.84 | 26.64 | 8.87 | 29.76 | 6 | 126 |
| 60 | 8.53 | 28.41 | 9.03 | 31.00 | 8 | 63 |
| 120 | 8.90 | 29.60 | 9.12 | 32.23 | 5 | 48 |
| 180 | 7.81 | 24.91 | 11.31 | 28.45 | 6 | 39 |
| 240 | 8.29 | 34.22 | 9.60 | 36.49 | 8 | 54 |
| 300 | 6.98 | 29.25 | 9.02 | 31.40 | 6 | 41 |

**Table 4**
RMS errors of radial, along track, cross track, and position for the batch least squares filter with various sampling periods.

| Sampling period (s) | Radial error (m, RMS) | Along error (m, RMS) | Cross error (m, RMS) | Position error (m, RMS) | Iteration # | Computing time (s) |
|---|---|---|---|---|---|---|
| 30 | 10.48 | 27.42 | 8.87 | 30.66 | 8 | 57 |
| 60 | 9.53 | 29.86 | 9.49 | 32.75 | 11 | 62 |
| 120 | 10.45 | 31.77 | 9.05 | 34.65 | 16 | 95 |
| 180 | N/A | N/A | N/A | N/A | N/A | N/A |
| 240 | N/A | N/A | N/A | N/A | N/A | N/A |
| 300 | N/A | N/A | N/A | N/A | N/A | N/A |

### 4.3. Effects of the measurement data-sampling periods

The comparisons of the non-recursive unscented batch filter with the batch least squares filter are carried out for six measurement data-sampling periods—30, 60, 120, 180, 240, and 300 s. The true initial position and velocity, the initial errors in position and velocity, and the initial covariance values of position and velocity errors are set to the same value as in Case-1 described in the previous subsection. In Table 3 and Table 4, the results are summarized for the radial, along track, cross track, positions errors, iteration number, and computing time for the non-recursive unscented batch filter and the batch least squares filter in the various sampling periods, respectively. In Figs. 5(a) and 5(b), the histories of iterations and initial estimate errors in position for the non-recursive unscented batch filter and the batch least squares filter are described for all six cases. When the sampling periods are 30, 60, and 120 s, the position accuracy of estimation yields a similar grade for both the filters. However, the batch least squares filter fails to get converged results when the sampling period is relatively large. When the sampling periods are longer (above 180 s) more advantages of the non-recursive unscented batch process become apparent. Generally, the computational efforts of the non-recursive unscented batch process are dependent on the total number of sigma points. So, the computational time of the non-recursive unscented batch filter is expected to be much more than that of the batch least squares filter. But for the 60 s and 120 s sampling periods, due to the decrease of iterations, the computational time for the non-recursive unscented batch algorithm is shorter than that of the batch least squares filter. Because both the two filters are used for post processing, the computational time is not a big issue. The two batch algorithms provide an estimate of the state at a chosen epoch using an entire set of data. So, long sampling periods may bring about a decline in accuracy due to the decrease of measurement data, as well as the nonlinear effect. According to Tables 3 and 4, and Figs. 5(a) and 5(b), the non-recursive unscented batch filter is converged robustly, and the position errors are kept at a similar level for all sampling periods. Especially, the adaptability to long sampling periods of the non-recursive unscented batch process is superior to the batch least squares filter.

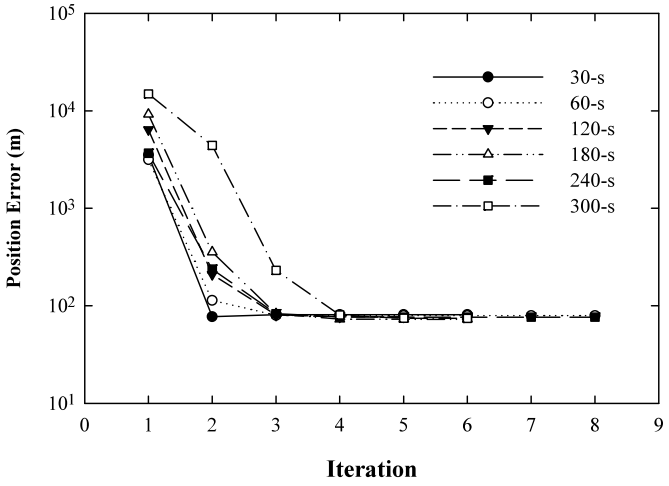

(a) non-recursive unscented batch filter

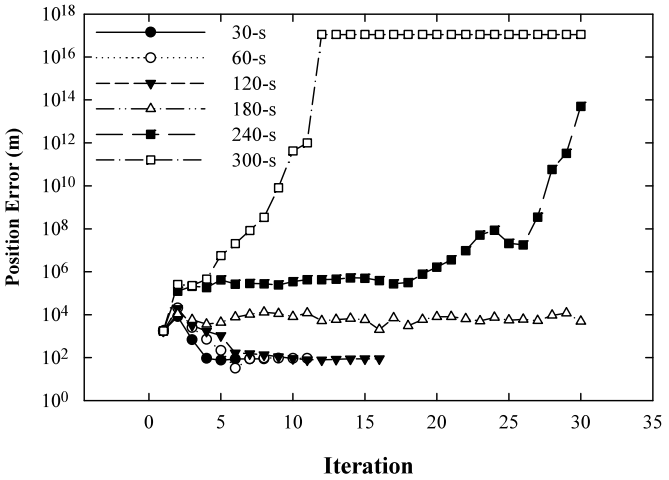

(b) batch least squares filter

**Fig. 5.** Histories of iterations and initial estimate errors in position for filters with various sampling periods.

### 4.4. Effects of the measurement errors

To examine the effects of measurement noise on the results, various levels of measurement noise are applied to the non-

**Table 5**
RMS errors of radial, along track, cross track, and position for the non-recursive unscented batch filter with various measurement noises.

| Case | Radial error (m, RMS) | Along error (m, RMS) | Cross error (m, RMS) | Position error (m, RMS) | Iteration # | Computing time (s) |
|---|---|---|---|---|---|---|
| 1 | 9.84 | 26.64 | 8.87 | 29.76 | 6 | 140 |
| 2 | 10.69 | 27.21 | 9.09 | 30.61 | 5 | 98 |
| 3 | 12.50 | 28.86 | 9.93 | 32.98 | 5 | 97 |
| 4 | 16.38 | 34.02 | 13.15 | 39.98 | 5 | 97 |
| 5 | 23.19 | 45.53 | 24.84 | 56.81 | 6 | 117 |
| 6 | 34.64 | 80.72 | 60.18 | 106.47 | 8 | 155 |

**Table 6**
RMS errors of radial, along track, cross track, and position for the batch least squares filter with various measurement noises.

| Case | Radial error (m, RMS) | Along error (m, RMS) | Cross error (m, RMS) | Position error (m, RMS) | Iteration # | Computing time (s) |
|---|---|---|---|---|---|---|
| 1 | 10.48 | 27.42 | 8.87 | 30.66 | 8 | 64 |
| 2 | 11.70 | 28.60 | 9.07 | 32.21 | 7 | 58 |
| 3 | 14.75 | 32.45 | 10.09 | 37.05 | 7 | 52 |
| 4 | 20.88 | 42.95 | 13.82 | 49.71 | 7 | 51 |
| 5 | 34.27 | 69.04 | 23.91 | 80.70 | 7 | 55 |
| 6 | 58.85 | 121.68 | 45.86 | 142.73 | 6 | 45 |

recursive unscented batch filter and the batch least squares filter. Six sets of standard deviations for range ($\sigma_{range}$), azimuth ($\sigma_{azimuth}$), and elevation ($\sigma_{elevation}$) errors assumed as [25 m, 0.015°, 0.015°] for Case-1, [50 m, 0.03°, 0.03°] for Case-2, [100 m, 0.06°, 0.06°] for Case-3, [200 m, 0.12°, 0.12°] for Case-4, [400 m, 0.24°, 0.24°] for Case-5, and [800 m, 0.48°, 0.48°] for Case-6. The noise characteristics of the three ground tracking stations are assumed to be the same. For each case, the measurement data are generated from the true orbit calculated by the HPOP as described in the subsection "Measurement data simulations and initial configurations." The initial conditions are assumed to be the same values as in the Case-1 described in the subsection "Effects of the initial errors in position and velocity." In Table 5 and Table 6, the results are summarized for the radial, along track, cross track, position errors, iteration number, and computing time for the non-recursive unscented batch filter and the batch least squares filter for various measurement noises, respectively. For the six test cases, the non-recursive unscented batch filter and the batch least squares filter are all converged within 5–9 iterations and both the filters are applicable for nonlinear estimation under noisy measurement. The number of iterations for the non-recursive unscented batch filter is less than those of the least squares filter. As can be seen in Table 5, Table 6, and Fig. 6, when the measurement noises are relatively small (Case-1 and Case-3), the position errors (the RMS position errors for 12 hours) from the non-recursive unscented batch filter are slightly better than the results of the batch least square filter. However, the larger the noise of measurement the better the results the non-recursive unscented batch filter achieves in terms of the RMS position accuracy.

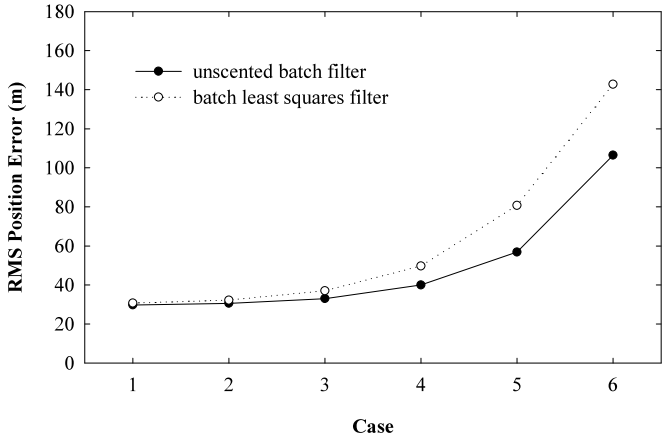


**Fig. 6.** RMS errors in position for various measurement noise levels for the non-recursive unscented batch filter and the batch least squares filter.

## 5. Conclusions

In the current paper, an alternative approach to batch algorithm, the non-recursive unscented batch filter using the unscented transformation, has been suggested and applied for satellite orbit determination. The system dynamic equations consist of the Earth's geo-potential, the atmospheric drag and the lunar/solar gravitational perturbations. The range, azimuth and elevation angle of the satellite measured from the ground stations are used for orbit determination. The purpose of the non-recursive unscented batch filter is to overcome the linearization and approximation errors. In the case of relatively small initial errors in position and velocity, or the short sampling periods of measurement data, or small measurement noises, results of the non-recursive unscented batch filter and the batch least squares filter are similar. But, as the nonlinearity is strengthened severely, in other words, as the large initial errors, long sampling periods and large measurement noises are considered, the non-recursive unscented batch process is more stable or needs fewer iterations for convergence or accurate than the batch least squares filter. Additionally, due to the unscented transformation, the calculations of partial derivatives are not required for the non-recursive unscented batch filter, which are very convenient to construct nonlinear estimation algorithms. Hence, the non-recursive unscented batch process can have an important role for verifying and improving other applications.

## Acknowledgements

This work is supported by the Korean Science and Engineering Foundation (KOSEF) through the National Research Laboratory. Program funded by the Ministry of Science and Technology (No. M10600000282-06J0000-28210).

## References

[1] Y. Bar-Shalom, X.-R. Li, T. Kirubarajan, Estimation with Applications to Tracking and Navigation, J. Wiley & Sons, New York, 2001.
[2] G.J. Bierman, Factorization Methods for Discrete Sequential Estimation, Academic Press, New York, 1977.
[3] A.E. Bryson, Y.C. Ho, Applied Optimal Control, Hemisphere Publishing Corp., Washington, DC, 1975.

[4] J.L. Crassidis, J.L. Junkins, Optimal Estimation of Dynamics Systems, Chapman & Hall/CRC, New York, 2004.
[5] J.L. Crassidis, F.L. Markley, Unscented filtering for spacecraft attitude estimation, Journal of Guidance, Control, and Dynamics 26 (4) (2003) 536–542.
[6] F. Daum, Nonlinear filters: Beyond the Kalman filter, IEEE Aerospace and Electronics Magazine 20 (8) (2005) 57–69.
[7] A. Farina, B. Ristic, D. Benvenuti, Tracking a ballistic target: Comparison of several nonlinear filters, IEEE Transaction on Aerospace and Electronics 38 (3) (2002) 854–867.
[8] D.C. Fraser, J.E. Potter, The optimum smoother as a combination of two optimum linear filters, IEEE Transaction on Automatic Control 14 (4) (1969) 387–390.
[9] D. Hobbs, P. Bohn, Precise orbit determination for low earth orbit satellites, Annals of the Marie Curie Fellowships 4 (2006) 128–135.
[10] S.J. Julier, J.K. Uhlmann, H.F. Durrant-Whyte, A new approach for filtering nonlinear systems, in: Proceedings of the American Control Conference, American Automatic Control Council, Evanston, IL, 1995, pp. 1628–1632.
[11] R.E. Kalman, A new approach to linear filtering and prediction theory, Journal of Basic Engineering E 82 (1) (1960) 35–45.
[12] D.-J. Lee, K.T. Alfriend, Adaptive sigma point filtering for state and parameter estimation, Paper No. AIAA 2004-5101, in: 2004 AIAA/AAS Astrodynamics Conference, Providence, RI, August 2004.
[13] D.-J. Lee, K.T. Alfriend, Sigma point filtering for sequential orbit estimation and prediction, Journal of Spacecraft and Rockets 44 (2) (2007) 388–398.
[14] O. Montenbruck, E. Gill, Satellite Orbits: Models, Methods, and Applications, Springer-Verlag, Berlin, 2000.
[15] M.L. Psiaki, Backward-smoothing extended Kalman filter, Journal of Guidance, Control, and Dynamics 28 (5) (2005) 885–894.
[16] M.L. Psiaki, M. Wada, Derivation and simulation testing of a sigma-points smoother, Journal of Guidance, Control, and Dynamics 30 (1) (2007) 78–86.
[17] K.-M. Roh, S.-Y. Park, E.-S. Park, K.-H. Choi, A batch filter based on the unscented transformation and its applications to spacecraft attitude determination, AAS 07-101, in: AAS/AIAA Space Flight Mechanics Meeting, Sedona, AZ, January 2007.
[18] STK, Satellite Tool Kit Software, Version 4.0, Analytical Graphics, Inc., Malvern, PA, 1998.
[19] B.D. Tapley, B.E. Schutz, G.H. Born, Statistical Orbit Determination, Elsevier Academic Press, Burlington, MA, 2004.
[20] D.A. Valado, Fundamentals of Astrodynamics and Applications, 2nd ed., Kluwer Academic Pub., Netherlands, 2001.
[21] E. Wan, R. van der Merwe, in: S. Haykin (Ed.), Kalman Filtering and Neural Networks, Wiley, New York, 2001.
[22] J.-C. Yoon, K.-H. Lee, B.-S. Lee, B.-Y. Kim, K.-H. Choi, Y.-K. Chang, Y.-S. Chun, S.-W. Ra, Geostationary orbit determination for time synchronization using analytical dynamic models, IEEE Transaction on Aerospace and Electronic System 40 (4) (2004) 1132–1146.
[23] S.-C. Zhang, S.-H. Liu, G.-D. Hu, Tracking a ballistic target with unscented iterative Kalman filter, in: Proceedings of the 31st Annual Conference of IEEE Industrial Electronics Society, Raleigh, NC, November 2005, pp. 107–111.

## Further reading

[24] E.J. Lefferts, F.L. Markley, M.D. Shuster, Kalman filtering for spacecraft attitude estimation, Journal of Guidance, Control, and Dynamics 5 (1982) 417–429.